Majority- and minority-spin-band directional Compton profiles in iron

1989 J. Phys.: Condens. Matter 1 9009

(http://iopscience.iop.org/0953-8984/1/45/023)

J. Phys.: Condens. Matter **1** (1989) 9009–9020. Printed in the UK

Majority- and minority-spin-band directional Compton profiles in iron

S P Collins†, M J Cooper†, D Timms†, A Brahmia†, D Laundy‡ and P P Kane§

† University of Warwick, Coventry CV4 7AL, UK
‡ SERC Daresbury Laboratory, Warrington WA4 4AD, UK
§ Indian Institute of Technology, Bombay 400076, India

Received 6 June 1989, in final form 24 July 1989

Abstract. Directional magnetic Compton profiles in BCC iron have been measured with circularly polarised 60 keV synchrotron radiation. Further measurements on iron, which are of improved statistical quality, enable majority and minority directional difference profiles to be separated and a more specific test of band theory to be made. The results are generally in good agreement with APW calculations, except in low-momentum regions, where there are significant discrepancies.

1. Introduction

Over the past few years a number of photon scattering experiments have been performed that make use of magnetic terms in the x-ray scattering cross section [1]. One of the most important of these is magnetic Compton scattering, which in its simplest form can be considered as the interaction between photons and the spin and charge of individual electrons. In contrast with the spatial distributions probed by diffraction studies, Compton scattering provides information about the electronic momentum distribution $n(p)$. The momentum distribution of the electrons involved in ferromagnetism is of particular interest, and it is precisely this that is isolated in a magnetic Compton scattering experiment.

1.1. Theory

The Compton profile, $J(p_z)$ is defined as a one-dimensional projection of the electron momentum distribution:

$$J(p_z) = \int\int (n_{\text{up}}(p) + n_{\text{down}}(p))\, \mathrm{d}p_x\, \mathrm{d}p_y \tag{1}$$

where p_x, p_y and p_z are the Cartesian momentum components, the z axis being parallel to the scattering vector (see [2] for a review of Compton scattering). It is related to the measured double-differential cross section by equation (2):

$$\mathrm{d}^2\sigma/\mathrm{d}\Omega\, \mathrm{d}E_2 = (\mathrm{d}\sigma/\mathrm{d}\Omega)(E_2/E_1)J(p_z) = r_0^2|A|^2(E_2/E_1)J(p_z) \tag{2}$$

where $\mathrm{d}\sigma/\mathrm{d}\Omega$ is the differential cross section, $E_{1(2)}$ the initial (final) photon energy, r_0

0953-8984/89/459009 + 12 $02.50

is the classical electron radius and A is proportional to the scattering amplitude. In the absence of any resonant effects this amplitude can be written [3, 4] as

$$A = a + \mathrm{i}\boldsymbol{b}\cdot\boldsymbol{S} + \mathrm{i}\boldsymbol{c}\cdot\boldsymbol{L} \tag{3}$$

where the first term is for charge scattering and is simply $\hat{\boldsymbol{e}}_1\cdot\hat{\boldsymbol{e}}_2$ (the Thomson term) when $E_1 \ll m_e c^2$ ($m_e c^2 \simeq 511$ keV). The second and third terms correspond to magnetic scattering from the electron spin $\boldsymbol{S}$ and orbital angular momentum $\boldsymbol{L}$ respectively, and are both smaller than the charge scattering amplitude by a factor of $\simeq E_1/m_e c^2$. The vectors $\boldsymbol{b}$ and $\boldsymbol{c}$ are determined by the photon energy and the scattering angle. In the present work the effects of orbital scattering can be neglected since the orbital moment in iron is very small. It is then clear from equation (3) that if $\boldsymbol{b}$ is real there is no interference between charge and magnetic scattering and $|A|^2$ contains only two contributions, namely, those from pure magnetic and charge scattering. The contribution from the magnetic term is therefore not only down in magnitude by a factor of $\simeq(E_1/m_e c^2)^2$ but also, as it is squared, the sign of $\boldsymbol{b}\cdot\boldsymbol{S}$ is lost, and with it any information relating to the electron spin direction. There is, however, an interference term if $\boldsymbol{b}$ is complex, and this corresponds physically to the incident photon beam having a non-zero degree of circular polarisation. Since the interference term is linear in $\boldsymbol{b}\cdot\boldsymbol{S}$ it is sensitive to the spin direction. It is therefore clear that magnetic Comptson scattering experiments require a beam of circularly polarised x-rays. Furthermore, since Compton scattering is an incoherent process, the technique is sensitive to spin directions summed over the electron distribution. Therefore only ferro- or ferrimagnetic materials can be studied, whereas in magnetic Bragg diffraction from antiferromagnets that restriction is absent [5].

It is convenient to remove the spin dependence from the differential cross section and re-write the double-differential cross section (equation (2)) in terms of 'total' and 'magnetic' Compton profiles

$$\mathrm{d}^2\sigma/\mathrm{d}\Omega\,\mathrm{d}E = (\mathrm{d}\sigma/\mathrm{d}\Omega)_{\mathrm{charge}}(E_2/E_1)J(p_z) + (\mathrm{d}\sigma/\mathrm{d}\Omega)_{\mathrm{mag}}(E_2/E_1)J_{\mathrm{mag}}(p_z) \tag{4}$$

where

$$J_{\mathrm{mag}}(p_z) = \int\int (n_{\mathrm{up}}(p) - n_{\mathrm{down}}(p))\,\mathrm{d}p_x\,\mathrm{d}p_y \tag{5}$$

and from the literature [6, 7, 8]

$$(\mathrm{d}\sigma/\mathrm{d}\Omega)_{\mathrm{mag}} = (-r_0^2/m_e c)P_c(1-\cos\Phi)\boldsymbol{S}\cdot(\boldsymbol{k}_1\cos\Phi + \boldsymbol{k}_2) \tag{6}$$

where P_c is the degree of circular polarisation of the incident beam, $\boldsymbol{k}_1$ and $\boldsymbol{k}_2$ are the incident and scattered wavevectors, Φ is the scattering angle and $\boldsymbol{S}$ is the polarisation of an electron in the 'up' state ($m_s = +\frac{1}{2}$). The magnetic Compton profile can then be obtained experimentally by subtracting data sets taken with the magnetising field direction or photon polarisation handedness reversed.

With an experimentally determined magnetic ($n_{\mathrm{up}} - n_{\mathrm{down}}$) Compton profile and a total ($n_{\mathrm{up}} + n_{\mathrm{down}}$) profile it is possible, in principle, to separate the Compton profiles of the majority and minority electrons. In practice, however, this is not straightforward as most of the electrons are unpolarised and contribute equally to both profiles. It will be shown later that this problem can be largely overcome by calculating the differences between profiles along various crystal directions.

1.2. Previous experimental work

The first magnetic Compton profile measurements were performed by Sakai and Ono [9, 10], who obtained circularly polarised γ-radiation from cryogenically oriented radioactive sources of ^{57}Co and ^{191}Ir. The γ-rays were scattered by a magnetised polycrystalline iron sample, and the magnetic profiles were isolated by subtracting data sets taken with opposite magnetic field directions. These pioneering experiments suffered from low count rates because only weakly active isotopes can be cooled effectively and the very long data collection times made such measurements far from routine.

Subsequent magnetic Compton experiments have differed significantly only in the source of circularly polarised radiation adopted. The two techniques used to date take advantage of the polarisation properties of synchrotron radiation. The first of these, the 'inclined view method', makes use of the fact that synchrotron radiation emitted at some small angle (typically a fraction of a milliradian) above or below the orbital plane is elliptically polarised [11] and therefore has some degree of circular polarisation, although reduced somewhat in intensity compared with radiation emitted in the plane. The feasibility of this method was first proposed by Holt and Cooper [11] and demonstrated by Holt and co-workers [12]. Subsequently, several experiments, including magnetic photoabsorption studies, have made use of this simple but effective technique for the extraction of circularly polarised synchrotron radiation [13, 14, 15].

In the second method, developed by Mills [16] from the method of Golovchenko and co-workers [17], an x-ray quarter-wave plate converts the linearly polarised radiation emitted in the orbital plane into elliptically polarised radiation. Each tailor-made plate can only be 'tuned' over a limited energy range.

The inclined view method currently gives the highest flux of circularly polarised radiation and it can be used over a very wide range of energies. Recently it has been adopted to measure magnetic Compton profiles along specific crystal directions in a single crystal of silicon-stabilised iron for the first time [18]. In the present paper the experiment is described in some detail and additional data of improved statistical quality are presented. The improvement is sufficient to allow the magnetic Compton profiles to be combined with previous total profiles to separate minority and majority contributions.

2. The magnetic Compton scattering experiment

A number of experimental parameters need to be determined in order to optimise the experiment and obtain the best data in the limited beam time available. Of these two of the most important and least obvious are the incident beam energy and the angle at which the synchrotron source is viewed. The choice of these parameters has been made much easier by utilising calculations of flux and circular polarisation by Laundy [19]. These calculations show (see figure 1) that on moving out of the orbital plane the degree of circular polarisation P_c increases from zero to almost unity, whilst the flux is correspondingly reduced from a maximum value on the axis to almost zero. There is clearly an optimum point between these two extremes.

In previous studies of magnetic Compton scattering with circularly polarised synchrotron radiation [12, 13] too much emphasis was put on maximising P_c, with consequent dramatic decreases in flux. The important quantity here is the signal-to-noise ratio, where the 'signal' is the weak magnetic signal which is proportional to P_cI (I is the scattered intensity) and the statistical noise comes from the dominant charge scattering

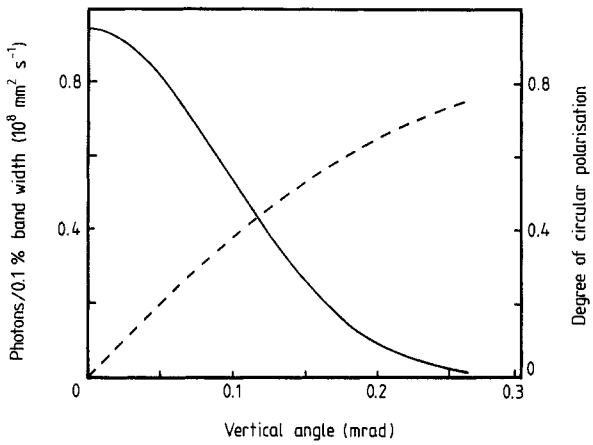

Figure 1. The predicted [19] variation of the brilliance (full curve, left-hand ordinate) and the degree of circular polarisation (broken curve, right-hand ordinate) as a function of the vertical angle of inclination to the synchrotron orbital plane. The calculations are for 60 keV photons on the SRS wiggler line 9.4.

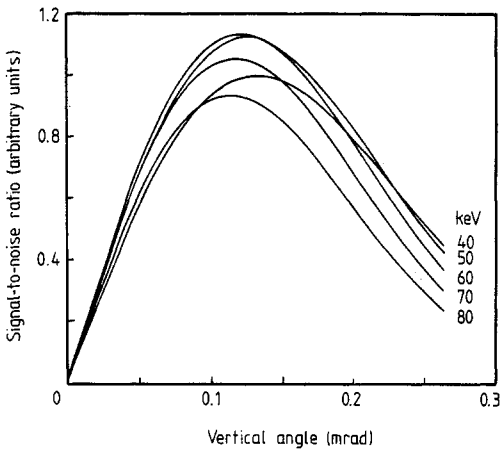

Figure 2. The magnetic signal-to-noise ratio in arbitrary units, as a function of the vertical angle of inclination from the synchrotron orbital plane for various incident photon energies. This calculation includes a simple correction for absorption in the iron sample.

which is proportional to $\sqrt{I}$. The signal-to-noise ratio is therefore proportional to $P_c\sqrt{I}$. This quantity depends critically on the incident beam energy, and there is a fairly narrow range of suitable energies. At low energies the magnetic term in the cross section becomes small (equation (6)), and the scattered intensity is reduced by the increase in photoelectric absorption. At higher energies the synchrotron flux falls rapidly, the monochromator efficiency is reduced, and due to the finite emittance (spread in position and velocity) of the circulating electron beam, the attainable degree of circular polarisation drops. The calculated signal/noise ratios (plotted in figure 2) predict that the optimum incident beam energy is between 50 and 60 keV. The magnetic Compton spectrometer was designed for energies in this range.

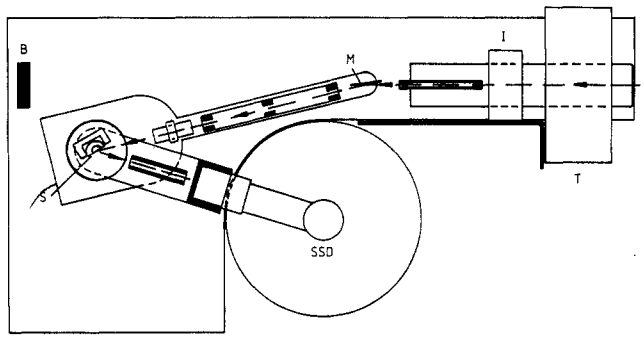

Figure 3. A schematic plan view of the magnetic Compton spectrometer. The radiation is collimated by a pair of finely adjusted tungsten slits (T). The intensity of the white beam is monitored by an ionisation chamber (I) then monochromated by a plane Ge 220 crystal (M). The radiation scattered by the magnetic sample (S) is detected by an intrinsic germanium solid-state detector (SSD). A lead beam stop (B) and extensive lead shielding are employed to remove stray radiation. The equipment is mounted on a platform that can be raised or lowered to select radiation emitted at different angles from the orbital plane.

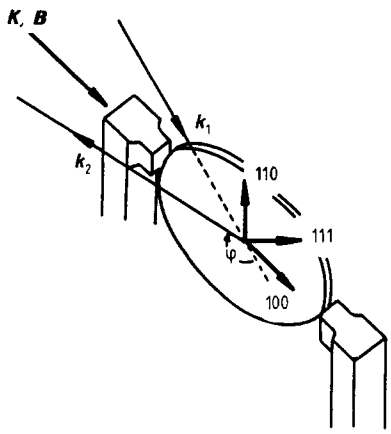

Figure 4. The scattering geometry for magnetic Compton measurements. A {110} single-crystal wafer of iron is clipped across the poles of an electromagnet. Each of the three main crystallographic axes may be brought into parallelism with the scattering vector, $\boldsymbol{K} = \boldsymbol{k}_1 - \boldsymbol{k}_2$ and the magnetisation direction, $\boldsymbol{B}$, by simply rotating the sample in its own plane. Note that although not shown in detail the pole pieces are shaped to ensure large scattering angles can be obtained.

The layout of the spectrometer is shown schematically in figure 3. White radiation from the 5 T SRS wiggler magnet, some 35 m distant, is incident on a mosaic Ge {110} monochromator 75 mm long, with the diffracted beam in the horizontal plane. At 60 keV the lowest-order (220) reflection had a Bragg angle of $\simeq 3°$ and an energy band width of $\simeq 0.15$ keV. This broadening is comparable to, but smaller than the energy resolution of the germanium solid-state detector employed in these measurements (FWHM $\simeq$ 0.36 keV at 60 keV), and therefore this approximate matching preserves the high monochromatic intensity with little deterioration in energy resolution of the experiment. The (440) reflection gives a 120 keV peak, but the harmonic flux is negligible because the critical energy of the wiggler is only 14 keV. It is worth noting that due to the very small Bragg angles involved, the monochromator has almost no effect on the circular polarisation of the x-ray beam.

Transmission scattering geometry was adopted for these directional measurements. At the expense of a small increase in absorption there are a number of major advantages over the more usual reflection geometry, which are evident from figure 4. Firstly, the

scattering vector and the magnetic field can be arranged to lie along the same direction in the plane of the thin sample; this gives nearly maximum magnetic scattering signal at large scattering angles. Secondly, if the cubic sample is a (110) single-crystal slice, then the three major crystal directions (100, 110 and 111) can all be found in its plane and oriented along the direction of the scattering vector and magnetic field by a simple rotation. The main disadvantage of this method is that the useful beam width is severely limited by the length of the sample since the projection onto the sample is magnified by a factor of approximately $\sec(\frac{1}{2}\Phi)$.

A scattering angle of 145° was chosen and a germanium SSD, 10 mm in diameter, was placed at approximately 220 mm from the sample. With an illuminated sample length of around 11 mm the finite range of scattering angles causes the profile to be smeared by a further 0.16 keV in addition to the broadening introduced by the detector and monochromator. The total momentum resolution of the spectrometer is 0.70 au (1 au = 1.99×10^{-24} kg m s^{-1}) with an incident beam energy of 58 keV.

The entire spectrometer, including the beam-defining slits and detector, is mounted on a substantial aluminium plate supported by four screw jacks. A single shaft drives the jacks simultaneously and allows the spectrometer to be moved vertically through a distance of several cm.

The ferromagnetic sample used throughout this work was a single-crystal disc of BCC iron grown by Metal Crystals Ltd, containing 6% of Si atoms to stabilise the BCC structure. The crystal was cut by spark erosion into a 25 mm disc of thickness $\simeq$0.25 mm, with the 110 crystal axis normal to the disc. The sample thickness was chosen in order to give the maximum scattered intensity in transmission, and the diameter was the largest that could be cut from the crystal.

The magnetic field direction and MCA data collection were controlled by a microcomputer which channelled data taken with each magnetic field direction into separate sections of memory. The magnetic field was flipped in an asynchronous cycle with a period of ten seconds in order to reduce the effects of any beam fluctuations. At the end of each run the two spectra were stored on magnetic disc and subtracted to obtain the magnetic Compton profile.

In order to optimise experimentally the signal-to-noise ratio in the magnetic profiles, a set of measurements of integrated Compton scattered flux and fractional magnetic effect were taken with the spectrometer at various heights above the orbital plane. With a vertical slit height of 5 mm the signal/noise ratio was found to be maximum with the centre of the slit $\simeq$6 mm above the orbital plane, corresponding to an angular range of 0.10 to 0.24 mrad. This is consistent with the calculations of Laundy [19], which predict the greatest signal/noise ratio with a narrow slit to be at $\simeq$0.14 mrad (figure 2).

With the spectrometer in this position the Compton count rate was around 10^3 s^{-1} with an average SRS beam current of $\simeq$150 mA. From this the flux of photons incident on the sample was estimated to be 7×10^6 s^{-1} mm^{-2}, i.e. $\simeq 10^8$ s^{-1} over a beam area of 3 mm horizontally by 5 mm vertically. The total data collection time for each crystal direction amounted to approximately 20, 8 and 14 h for the 100, 110 and 111 directions respectively, with a typical run lasting 6 h. This gave integrated intensities of $(40\text{–}80) \times 10^6$ Compton counts, which represents an increase of around a factor of four over the previous measurements [18]. The overall size of the magnetic effect, given by the difference in Compton count rate for the two field directions divided by their sum, was measured to be 0.95%. From a comparison with the magnetic and non-magnetic parts of the cross section [6], this value indicates an average degree of polarisation of $P_c \simeq 0.45$, which is consistent with the calculation shown in figure 1.

3. Data processing

Data sets from each run were analysed separately in order to check their consistency and allow for any small changes in beam energy or scattering angle. The data processing required for magnetic Compton profiles is simpler than for non-magnetic data since many of the systematic errors are reduced or eliminated (i.e. background contributions) in the magnetic difference experiments. The larger statistical errors also mean that small corrections are insignificant.

The data were corrected firstly for the low-energy tail of the detector response, and then for the variation in sample absorption and magnetic cross section across the profile. The profile areas were normalised to 2.2 (the number of unpaired electrons in iron) in the momentum range -8 to $+8$ au, and the data were averaged in momentum intervals of 0.2 au. After checking for symmetry, the profiles were folded about $p_z = 0$, providing final profiles for each data set. The folding process eliminates the dominant linear part of the absorption and cross section corrections, so these had very little effect on the final profiles.

The effect of multiple scattering in magnetic Compton measurements has been considered by Sakai [20], who performed Monte Carlo simulations of multiple scattering from a thick iron sample in reflection geometry and with an incident beam energy of 60 keV. Since the sign of the magnetic form is opposite for forward- and back-scattering, there is a cancellation effect in the magnetic multiple scattering and therefore the ratio of multiple to single scattering is lower than for the non-magnetic case. The results of the simulation show that the multiple-scattering contribution to the data from this thin sample is negligible when compared with statistical errors. Although a full simulation of the present experiment would be required for a point-by-point correction, estimates show that the small multiple-scattering contribution is of a similar shape to the single-scattering profile, and the consequent effect on the renormalised lineshape was insignificant. The effects of multiple scattering were therefore neglected. The final magnetic Compton profile for each of the three crystal directions is shown in figure 5 and presented numerically in table 1.

By combining the magnetic Compton profiles (equation (5)) with total profiles (equation (1)), contributions from the majority and minority electrons can be obtained separately. The two profiles look very similar, however, since they are dominated by the same core contributions. The contributions from tightly bound core electrons could be eliminated by subtracting calculated atomic profiles from the data. This would be strongly affected by any systematic errors in the data processing procedure of either the magnetic and non-magnetic profiles, which is not desirable. A more satisfactory technique is to consider differences between profiles measured along various crystal directions. This method is commonly adopted in the analysis of non-magnetic Compton profile data [2]. If the charge and magnetic directional difference profiles are defined as

$$\Delta J_{\text{charge}}(p_z) = J^1_{\text{charge}}(p_z) - J^2_{\text{charge}}(p_z) \tag{7}$$

and

$$\Delta J_{\text{mag}}(p_z) = J^1_{\text{mag}}(p_z) - J^2_{\text{mag}}(p_z) \tag{8}$$

where the superscripts 1 and 2 refer to two different crystal directions, it follows that

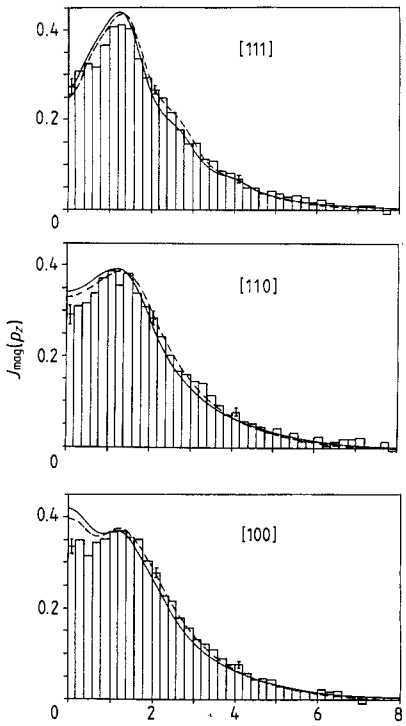

Figure 5. The measured directional magnetic Compton profiles (listed in table 1) and the APW [28] (full curve) and LMTO [29] (broken curve) theoretical profiles plotted as a function of the electron momentum ($1\ \text{au} = 1.99 \times 10^{-24}\ \text{kg m s}^{-1}$). The latter have been convoluted with a Gaussian of FWHM 0.70. au to match the experimental resolution and all profiles have been normalised to an area of 2.2 electrons in the momentum range −8 to +8 au.

directional difference profiles for the majority and minority electrons can be obtained separately from

$$\Delta J_{\text{maj}}(p_z) = \tfrac{1}{2}(\Delta J_{\text{charge}}(p_z) - \Delta J_{\text{mag}}(p_z)) \tag{9}$$

and

$$\Delta J_{\text{min}}(p_z) = \tfrac{1}{2}(\Delta J_{\text{charge}}(p_z) + J_{\text{mag}}(p_z)). \tag{10}$$

The non-magnetic difference profiles could in principle be obtained from the same raw data as the magnetic profiles, and this would obviously have the advantage that the profiles have the same energy resolution. Unfortunately, due to small changes in the relatively large background associated with synchrotron experiments, this method is not reliable with the present data. Instead, data from previous (higher-resolution) γ-ray measurements [21, 22] were used, after convoluting with a Gaussian to match the 0.70 au resolution of the synchrotron data. The results of the directional differences are shown in figure 6.

4. Discussion

All measurements described in this paper concern SiFe, with ≈6% Si atoms at interstitial lattice sites. As spin-polarised band-structure calculations for SiFe have not been performed, we assume that the electronic structure is unaffected by the Si.

In common with the magnetic Compton profile measurements on polycrystalline samples [9, 12, 23], the directional profiles (figure 5) are characterised by central dips,

Table 1. Directional magnetic Compton profiles of iron. Tabulated values of the magnetic Compton profiles $J(p_z)$ are averages of data points in the momentum ranges p_z to $(p_z + 0.2)$ au and $-p_z$ to $-(p_z + 0.2)$ au. Experimental errors in the last digit(s) are shown in brackets. The momentum resolution is 0.70 au.

	$J(p_z)$				$J(p_z)$		
p_z	100	110	111	p_z	100	110	111
0.0	0.334(15)	0.289(22)	0.273(17)	5.0	0.031	0.042	0.035
0.2	0.347	0.307	0.308	5.2	0.026	0.026	0.028
0.4	0.313	0.315	0.325	5.4	0.023	0.031	0.032
0.6	0.342	0.337	0.317	5.6	0.021	0.012	0.027
0.8	0.352	0.371	0.366	5.8	0.013	0.017	0.017
1.0	0.368	0.387	0.408	6.0	0.024(5)	0.022(8)	0.023(5)
1.2	0.370	0.355	0.411	6.2	0.020	0.001	0.016
1.4	0.353	0.381	0.401	6.4	0.020	0.011	0.010
1.6	0.349	0.337	0.336	6.6	0.008	0.018	0.010
1.8	0.303	0.309	0.293	6.8	0.005	0.018	0.007
2.0	0.277(10)	0.284(14)	0.266(11)	7.0	−0.002	0.022	0.010
2.2	0.226	0.242	0.249	7.2	0.006	0.003	0.011
2.4	0.216	0.199	0.216	7.4	0.003	0.000	0.004
2.6	0.179	0.166	0.178	7.6	0.004	0.013	−0.006
2.8	0.156	0.161	0.147	7.8	0.006	−0.001	0.003
3.0	0.131	0.144	0.149	8.0	0.001(4)	−0.004(6)	0.001(5)
3.2	0.122	0.140	0.111	8.2	0.003	0.008	−0.001
3.4	0.111	0.113	0.108	8.4	0.010	0.003	0.009
3.6	0.092	0.092	0.085	8.6	0.000	0.001	0.006
3.8	0.077	0.070	0.082	8.8	−0.005	0.001	0.000
4.0	0.078(7)	0.078(9)	0.067(7)	9.0	0.005	0.006	0.007
4.2	0.061	0.056	0.048	9.2	0.008	0.009	−0.001
4.4	0.044	0.052	0.049	9.4	0.001	−0.003	0.003
4.6	0.047	0.044	0.035	9.6	0.017	0.012	0.002
4.8	0.043	0.035	0.041	9.8	0.003	−0.004	0.003

giving the familiar 'volcano' structure. The dips arise from regions in momentum space where the density $n(p)$ of the majority-band electrons is smaller than that of the minority band. This reversed polarisation at low momentum has also been observed in spin-polarised positron annihilation experiments [24], and is due to the low-momentum s–p conduction electrons having opposite polarisation to those in the more localised 3d band [25]. This interpretation is consistent with observations of regions in real space of reversed polarisation between atomic sites in polarised neutron diffraction experiments [26].

The main differences between the three directional magnetic profiles are in the sizes of the central dip, which is smallest in the 100 profile and largest in 111. This can be understood qualitatively from the shapes of the Fermi surfaces. At the centre of the profile the contributing wavevectors must all lie in a plane perpendicular to the scattering vector, which passes through the centre of the Brillouin zone (the Γ-point). The majority and minority Fermi surfaces that intersect these 'slices' through the Brillouin zone have been calculated by Tawil and co-workers [27]. It can be seen that the majority band shows smaller anisotropies associated with the Fermi surface cross sections indicating that the directional features are associated mainly with the minority band [21]. One of the most notable differences between the minority and majority Fermi surfaces is that

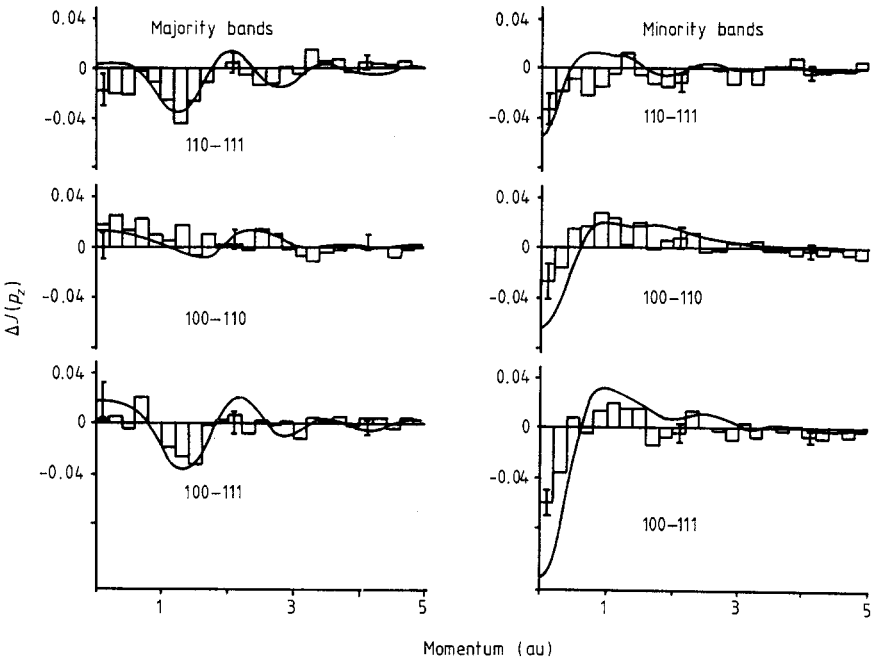

Figure 6. The majority- and minority-band directional difference profiles, as defined by equations (7)–(10), of ferromagnetic iron. The full curves represent an APW calculation [28] which has been convoluted with the experimental resolution function of 0.70 au FWHM.

the former has large holes at the H points, whereas the latter does not. As such holes in the minority band contribute positively to the profile, one might expect the 100 profile, which has the most H points, to be largest at the centre, and the 111, which has none, to be smallest. This is indeed what is found, although too much weight should not be attached to this speculative description.

The directional magnetic Compton profiles have been compared quantitatively with the results of APW [28] and LMTO [29] calculations. The APW calculations were based on the method described in [25], except that the momentum density was calculated out to 7 atomic units of momentum rather than the original 5 au, in order to improve the high-momentum part of the profiles. The LMTO calculations are described in [30]. The parametrised version was adopted in preference to the self-consistent calculation as the latter was forced to reproduce more accurately the Fermi surface topology and magnetic moment, although the profiles from each method were very similar. The calculated profiles agree well with the measurements along the 110 and 111 directions, but both predict a small central peak in the 100 profile, in contrast with the small dip observed in the experimental data. This would explain why the data on polycrystalline iron [23] also show a larger central dip than the calculation.

Although the directional difference profiles for the minority and majority bands formed according to equations (9) and (10) are of quite poor statistical quality, they demonstrate the great sensitivity of such measurements, which is likely to be very important in future, more precise studies. The APW calculation gives results very close to the data above 1 au, and the main discrepancies appear at low momentum. In the majority band the predictions for the 100–111 and 110–111 profiles are too high, and the

minority band has the 100–110 and 100–111 calculations too low. These features cannot be interpreted unambiguously in terms of the individual profiles along each direction but from figures 5 and 6 it seems likely that the 100 and 110 calculated majority profiles are too large at low momenta, whereas in the minority band the 100 calculation is too small. It is impossible to pinpoint the source of discrepancy from these data alone. Further model calculations are required in order to determine which features of the band structure are responsible for the Compton profile differences at low momentum.

It is assumed that a few per cent of Si added to the Fe do not greatly affect the spin-dependent electronic structure, but this should be further investigated. It is not only interesting in its own right, but also a common problem with experiments that require large crystals of BCC Fe. Systematic studies of SiFe crystals with varying percentages of Si, along with band calculations for random SiFe alloys, should shed light on this problem. Recent measurements of the directional Compton profiles of pure nickel by the present authors show similar deviations from APW theory, which suggests that the discrepancies seen here have a more general origin.

With the present experimental arrangement, magnetic Compton profiles of systems with large moments (i.e. $\mu \geqslant 2\,\mu_B$) can be measured routinely, and require data collection times typically of a few days. In order to extend these measurements to systems with smaller moments, a significant increase in incident beam intensity is required. In the future this will be achieved by the use of a horizontally focusing monochromator at the same beam line station. It is envisaged that a gain in intensity of at least an order of magnitude will be possible, greatly increasing the range of interesting magnetic materials that can be studied by this new technique.

Acknowledgments

We are indebted to the SERC for research grants and beam time allocation at the Daresbury Storage Ring Source. We are grateful to Dr G Clark of the Daresbury Laboratory for practical help and advice.

References

[1] Cooper M J 1989 *Physica* **3159** 137
[2] Cooper M J 1985 *Rep. Prog. Phys.* **48** 45
[3] Platzman P M and Tzoar N 1985 *J. Appl. Phys.* **57** 3623
[4] Gell-Mann M and Goldberger M L 1954 *Phys. Rev.* **96** 1433
[5] Bergevin F De and Brunel M 1972 *Phys. Lett.* **39A** 141
[6] Lipps F W and Tolhoek H A 1954 *Physica* **30** 395
[7] Lovesey S W 1987 *J. Phys. C: Solid State Phys.* **20** 5625
[8] Blume M and Gibbs D 1988 *Phys. Rev.* B **37** 1779
[9] Sakai N and Ono K 1976 *Phys. Rev. Lett.* **37** 351
[10] Sakai N, Terashima O and Sekizawa H 1984 *Nucl. Instrum. Methods* **221** 419
[11] Holt R S and Cooper M J 1983 *Nucl. Instrum. Methods* **213** 447
[12] Holt R S, Laundy D, Cardwell D A, Cooper M J, Naylor T, Manninen S and Hatton P 1986 *Nucl. Instrum. Methods* A **243** 608
[13] Cooper M J, Laundy D, Cardwell D A, Timms D N, Holt R S and Clark G 1986 *Phys. Rev.* B **34** 5984
[14] Schutz G, Wagner W, Wilhelm W, Kiendle P, Zeller R, Frahm R and Materlik G 1987 *Phys. Rev. Lett.* **58** 737
[15] Collins S P, Cooper M J, Brahmia A, Laundy D and Pitkanen T 1989 *J. Phys. Condens. Matter* **1** 323
[16] Mills D M 1987 *Phys. Rev.* B **36** 6178

[17] Golovchenko J A, Kincaid B M, Levesque R A, Meixner A E and Kaplan D R 1986 *Phys. Rev. Lett.* **57** 202
[18] Cooper M J, Collins S P, Timms D N, Brahmia A, Kane P P, Holt R S and Laundy D 1988 *Nature* **333** 151
[19] Laundy D 1989 *Daresbury Laboratory Preprint*, submitted to *Nucl. Instrum. Methods*
[20] Sakai N 1987 *J. Phys. Soc. Japan* **56** 2477
[21] Rollason A J 1984 *PhD Thesis* University of Warwick
[22] Rollason A J, Holt R S and Cooper M J 1983 *J. Phys. F: Met. Phys.* **13** 1807
[23] Timms D N, Brahmia A, Collins P, Collins S P, Cooper M J, Holt R S, Kane P P, Clark G and Laundy D 1988 *J. Phys. F: Met. Phys.* **18** L57
[24] Mijnarends P E 1973 *Physica* **63** 248
[25] Wakoh S and Kubo Y 1977 *J. Magn. Magn. Mater.* **5** 202
[26] Shull C G and Yamada Y 1962 *J. Phys. Soc. Japan Suppl.* B III **17** 1
[27] Tawil R A and Callaway J 1973 *Phys. Rev.* B **7** 4242
[28] Wakoh S 1988 private communication.
[29] Singh A K and Genoud P 1988 private communication
[30] Genoud P, Singh A K, Manuel A A, Jarlborg T, Walker E, Peter M and Weller M 1988 *J. Phys. F: Met. Phys.* **18** 1933